

1 **Evaluation of water flux predictive models developed using eddy** 2 **covariance observations and machine learning: a meta-analysis**

3 Haiyang Shi^{1,2,4,5}, Geping Luo^{1,2,3,5}, Olaf Hellwich⁶, Mingjuan Xie^{1,2,4,5}, Chen Zhang^{1,2}, Yu Zhang^{1,2}, Yuangang
4 Wang^{1,2}, Xiuliang Yuan¹, Xiaofei Ma¹, Wenqiang Zhang^{1,2,4,5}, Alishir Kurban^{1,2,3,5}, Philippe De Maeyer^{1,2,4,5} and
5 Tim Van de Voorde^{4,5}

6
7 ¹ State Key Laboratory of Desert and Oasis Ecology, Xinjiang Institute of Ecology and Geography, Chinese
8 Academy of Sciences, Urumqi, Xinjiang, 830011, China.

9 ² University of Chinese Academy of Sciences, 19 (A) Yuquan Road, Beijing, 100049, China.

10 ³ Research Centre for Ecology and Environment of Central Asia, Chinese Academy of Sciences, Urumqi, China.

11 ⁴ Department of Geography, Ghent University, Ghent 9000, Belgium.

12 ⁵ Sino-Belgian Joint Laboratory of Geo-Information, Ghent, Belgium and Urumqi, China.

13 ⁶ Department of Computer Vision & Remote Sensing, Technische Universität Berlin, 10587 Berlin, Germany.

14
15 **Correspondence to: Geping Luo (luogp@ms.xjb.ac.cn) and Olaf Hellwich (olaf.hellwich@tu-berlin.de)**

16 Submitted to *Hydrology and Earth System Sciences*

17 **Abstract.**

18 With the rapid accumulation of water flux observations from global eddy-covariance flux sites, many studies
19 have used data-driven approaches to model site-scale water fluxes with various predictors and machine learning
20 algorithms used. However, systematic evaluation of such models is still limited. We therefore performed a meta-
21 analysis of 32 such studies, derived 139 model records, and evaluated the impact of various features on model
22 accuracy throughout the modeling flow. SVM (average R-squared = 0.82) and RF (average R-squared = 0.81)
23 outperformed over evaluated algorithms with sufficient sample size in both cross-study and intra-study (with the
24 same training dataset) comparisons. The average accuracy of the model applied to arid regions is higher
25 than in other climate classes. The average accuracy of the model was slightly lower for forest sites
26 (average R-squared = 0.76) than for cropland and grassland sites (average R-squared = 0.8
27 and 0.79), but higher than for shrubland sites (average R-squared = 0.67). Among various predictor
28 variables, the use of net/sun radiation Using Rn/Rs, precipitation, air temperature Ta, and the fraction of absorbed
29 photosynthetically active radiation FAPAR improved the model accuracy. Among the different validation
30 methods, random The combined use of Ta and Rn/Rs is very effective especially in forests, while in grasslands
31 the combination of Ws and Rn/Rs is also effective. Random cross-validation shows showed higher model
32 accuracy than spatial cross-validation and temporal cross-validation, but spatial cross-validation is more
33 important for the application for water flux predictive models when used for in spatial extrapolation. The
34 findings of this study are promising to guide future research on such machine learning-based modeling.

35 **1 Introduction**

36 Evapotranspiration (ET) is one of the most important indicator components of the water cycle in terrestrial
37 ecosystems. It also represents the key variable in linking ecosystem functioning, carbon and climate feedbacks,
38 agricultural management, and water resources (Fisher et al., 2017). The quantification of ET for regional,
39 continents, or the globe can improve our understanding of the water, heat, and carbon interactions, which is
40 important for global change research (Xu et al., 2018). Information on ET has been used in many fields,
41 including, but not limited to, droughts and heatwaves (Miralles et al., 2014), regional water balance closures
42 (Chen et al., 2014; Sahoo et al., 2011), agricultural management (Allen et al., 2011), water resources
43 management (Anderson et al., 2012), biodiversity patterns (Gaston, 2000). In addition, accurate large-scale and
44 long-time series ET prediction at high spatial and temporal resolution has been of great interest (Fisher et al.,
45 2017).

46
47 Currently, there are three main approaches for simulation and spatial and temporal prediction of ET: (i) physical
48 models based on remote sensing such as surface energy balance models (Minacapilli et al., 2009; Wagle et al.,
49 2017), Penman-Monteith equation (Mu et al., 2011; Zhang et al., 2010), Priestley-Taylor equation (Miralles et
50 al., 2011); (ii) process-based land surface models, biogeochemical models and hydrological models (Barman et
51 al., 2014; Pan et al., 2015; Sándor et al., 2016; Chen et al., 2019); and (iii) the observation-based machine
52 learning modeling approach with in situ eddy covariance (EC) observations of water flux (Jung et al., 2011; Li
53 et al., 2018; Van Wijk and Bouten, 1999; Xie et al., 2021; Xu et al., 2018; Yang et al., 2006; Zhang et al., 2021).
54 For remote sensing based physical models and process based land surface models, some physical processes

55 have not been well characterized due to the lack of understanding of the detailed mechanisms influencing ET
56 under different environmental conditions (Jung et al., 2011; Li et al., 2018; Van Wijk and Bouten, 1999; Xie et
57 al., 2021; Xu et al., 2018; Yang et al., 2006; Zhang et al., 2021). For remote sensing-based physical models and
58 process-based land surface models, some physical processes have not been well characterized due to the lack of
59 understanding of the detailed mechanisms influencing ET under different environmental conditions. For
60 example, the inaccurate representation and estimation of stomatal conductance (Li et al., 2019) and the
61 linearization (McColl, 2020) of the Clausius-Clapeyron relation in the Penman-Monteith equation may
62 introduce both empirical and conceptual errors into estimates of ET. Limited by complicated assumptions and
63 model parametrizations, these process-based models face challenges in the accuracy of their ET estimations over
64 heterogeneous landscapes (Pan et al., 2020; Zhang et al., 2021). Therefore, many researchers have used data-
65 driven approaches for the simulation and prediction of ET with the accumulation of a large volume of measured
66 site-scale observational data of water fluxes in the past decades. Various machine learning models have been
67 developed to simulate water fluxes at the flux site scale. Besides, various predictor variables (e.g.,
68 meteorological factors, vegetation conditions, and moisture supply conditions) have been incorporated into such
69 models for upscaling (Fang et al., 2020; Jung et al., 2009) of water flux to a larger scale or understanding the
70 driving mechanisms with the variable importance analysis performed in such models.

71
72 However, to date, the systematic assessment of the uncertainty in the processes of water flux prediction models
73 constructed using the machine learning approach is limited. Although considerable effort has been invested in
74 improving the accuracy of such prediction models, our understanding of the expected accuracy of such models
75 under different conditions is still limited. It is still not easy for us to give the general guidelines for selecting
76 appropriate predictor variables and models. Questions such as ‘Which predictor variables are the best in water
77 flux simulations?’ and ‘How to improve the prediction accuracy of water flux effectively?’ etc. still confuse the
78 researchers in the field. Therefore, we should synthesize the findings from published ~~such~~ studies to determine
79 which predictor variables, machine learning models, and other features can significantly improve the prediction
80 accuracy of water flux. Also, we are interested in understanding under which specific conditions they are more
81 effective.

82
83 A variety of features ~~may affect~~ control the accuracy of such models, including the predictor variables used, the
84 inherent heterogeneity within the dataset, the plant functional type (PFT) of the flux sites, the method of model
85 construction and validation, and the ~~machine-learning~~ algorithm chosen:

- 86 a) Predictor variables used: Compared to process-based models, ~~the~~ data used may have a more significant
87 impact on the final model performance in data-driven models. Various biophysical covariates and other
88 environmental factors have been used for the simulation and prediction of water fluxes. The most
89 commonly used factors include mainly precipitation (Prec), air temperature (Ta), wind speed (Ws), net/sun
90 radiation (Rn/Rs), soil temperature (Ts), soil texture, vapor-pressure deficit (VPD), the fraction of absorbed
91 photosynthetically active radiation (FAPAR), vegetation index (e.g., [Normalized Difference Vegetation
92 Index \(NDVI_r\)](#), [Enhanced Vegetation Index \(EVI_r\)](#)), [Leaf area index \(LAI_r\)](#), and carbon fluxes (e.g.,
93 [Gross Primary Productivity \(GPP_r\)](#)). These used predictor variables and their complex interactions drive
94 the fluctuations and variability of water fluxes. They affect the accuracy of water flux simulations in two

95 ways: their actual impact on water fluxes at the process-based level and their spatio-temporal resolution and
96 inherent accuracy. The relationship between water fluxes and these variables at the process-based driving
97 mechanism level is very different under different PFTs, different climate types, and different
98 hydrometeorological conditions. For example, in irrigated croplands in arid regions, water fluxes may be
99 highly correlated with irrigation practices, and thus soil moisture may be a very important predictor
100 variable, and its importance may be significantly higher than in other PFTs. And in models that incorporate
101 data from multiple PFTs, some variables that play important roles in multiple PFTs may have higher
102 importance. In terms of data spatial and temporal resolution, the data for these predictor variables may have
103 different scales. In terms of spatial resolution, meteorological observations such as precipitation and air
104 temperature are at the flux site scale, while factors extracted from satellite remote sensing and reanalysis
105 climate datasets cover a much larger spatial scale (i.e. the grid-scale). This leads to considerable differences
106 in the degree of spatial match between different variables and the site scale EC observations (approximately
107 100 m x 100 m). It is therefore difficult for some variables to be fairly compared in the subsequent
108 importance analysis of driving factors. In terms of temporal resolution, the importance of predictor
109 variables with different temporal resolutions may be variable for models with different time scales (e.g.,
110 half-hourly, daily, and monthly models). For example, the daily or 8-day NDVI data based on MODIS
111 satellite imagery may better capture the temporal dynamics of water fluxes concerning vegetation growth
112 than the 16-daily NDVI data derived from Landsat images. Besides, data on non-temporal dynamic
113 variables such as soil texture cannot explain temporal variability in water fluxes in the data-driven
114 simulations, although soil texture may be important in the interpretation of the actual driving mechanisms
115 of ET (which may need to be quantified in detail in ET simulations by process-based models). In addition,
116 some inherent accuracy issues (e.g., remote sensing-based NDVI may not be effective at high values) of the
117 predictors may propagate into the consequent machine learning models, thus affecting the modeling and our
118 understanding of its importance. Therefore, it is necessary to consider the spatial and temporal resolution of
119 the data and their inherent accuracy for the predictors used in different studies in the systematic evaluation
120 of data-driven water flux simulations.

121 b) ~~The volume of the dataset, inherent~~ heterogeneity of the dataset, and ~~how the model is validated~~ validation:
122 the volume and inherent spatiotemporal heterogeneity of the training dataset (with more variability and
123 extremes incorporated) may affect model accuracy. Typically, training data with larger regions, multiple
124 sites, multiple PFTs, and longer year spans may have a higher degree of imbalance (Kaur et al., 2019; Van
125 Hulse et al., 2007; Virkkala et al., 2021; Zeng et al., 2020)(Kaur et al., 2019; Van Hulse et al., 2007;
126 Virkkala et al., 2021; Zeng et al., 2020). And in machine learning, in general, modeling with unbalanced
127 data (with significant differences in the distribution between the training and validation sets) may result in
128 lower model accuracy. Currently, the most common ways of model validation include spatial, temporal, and
129 random cross-validation. Spatial validation is mainly to evaluate the ability of the model to be applied in
130 different regions or flux sites with different PFT types, and one of the common methods is 'leave one site
131 out' (Fang et al., 2020; Papale et al., 2015; Zhang et al., 2021). If the data of the site left out for validation
132 differs significantly from the distribution of the training data set, the expected accuracy of the model
133 applied at that site may be low because the trained model may not capture the specific and local
134 relationships between the water flux and the various predictor variables at that site. For temporal validation,

135 to assess the ability of the models to adapt to the interannual variability, typically some years of data are
136 used for training and the remaining years for model validation (Lu and Zhuang, 2010). If a year with
137 extreme climate is used for validation, the accuracy may be low because the training dataset may not
138 contain such extreme climate conditions. In the case of PFTs that are significantly affected by human
139 activities, such as cropland, the possible different crops grown and different land use practices (e.g.,
140 irrigation) across years can also lead to low accuracy in temporal validation. ~~K-fold cross-validation is
141 commonly used in random cross-validation to assess the fitness of the model to the spatio-temporal
142 variability. In this case, different values of K may also affect the model accuracy. For example, for an
143 unbalanced dataset, the average model accuracy obtained from a 10-fold (K = 10) validation approach is
144 likely to be higher than that of a 3-fold (K = 3) validation approach.~~

145 c) Various machine learning algorithms: Some machine learning algorithms may have specific advantages
146 when applied to model the relationships between water fluxes and covariates. For example, neural networks
147 may have an advantage in nonlinear fitting, while random forests ~~may can~~ avoid ~~serious~~ overfitting ~~due to~~
148 ~~the introduction of randomness problems~~. However, which algorithm is better overall in different situations
149 (i.e. applied to different data sets)? Which algorithm is generally more accurate than the others when using
150 the same data set? A comprehensive evaluation ~~of this is necessary, important.~~

151
152 Therefore, to systematically and comprehensively assess the impact of various features in such modeling, we
153 perform a meta-analysis of published water flux simulation studies that combine the flux site water flux
154 observations, various predictors, and machine learning. The accuracy of model records collected from the
155 literature was linked with various model features to assess the impacts of predictor data types, algorithms, and
156 other features on model accuracy. The findings of this study may be promising to improve our understanding of
157 the impact of various features of the models to guide future research on such machine learning-based modeling.

158 2 Methodology

159 2.1 Protocol for selecting the sample of articles

160 We applied a general query (on December 1st, 2021) on title, abstract, and keywords to include articles with the
161 “OR” operator applied among expressions (Table 1) in the Scopus database. Preferred Reporting Items for
162 Systematic Reviews and Meta-Analyses (PRISMA) (Moher et al., 2009) ~~is are~~ followed when filtering the
163 papers. ~~We first excluded articles that obviously did not fit the topic of this study based on the abstract, and then
164 performed the article screening with the full-text reading.~~

165
166 The inclusion of articles follows the following criteria:

- 167 a) Articles were filtered for those with water fluxes (or latent heat) simulated, ~~with multi-variable,~~
- 168 b) The water flux or latent heat observations used in the prediction models should be from the eddy-
169 covariance flux measurements.
- 170 c) Articles focusing only on gap-filling (Hui et al., 2004) techniques (i.e., the objective was not simulation
171 and extrapolation of water fluxes using machine learning) were excluded.

设置了格式: 字体: 10 磅, 加粗

带格式的: 标题 2, 行距: 单倍行距

- 172 d) Only articles that used multivariate regression used, (with the number of covariates greater than or equal to
 173 3) were included.
- 174 e) The determination coefficient (R-squared) of the validation step should be reported as the metric of model
 175 performance (Shi et al., 2021; Tramontana et al., 2016; Zeng et al., 2020), and published in English
 176 journals. (Shi et al., 2021; Tramontana et al., 2016; Zeng et al., 2020) in the articles.
- 177 f) The articles should be published in English-language journals.

178

179 Although RMSE is also often used for model accuracy assessment, its dependence on the magnitude of water
 180 flux values makes it difficult to use for fair comparisons between studies. For example, due to the difference in
 181 the range of ET values, models developed from flux stations in dry grasslands will typically have lower RMSE
 182 than models developed by flux stations based on forests in humid regions. Therefore, RMSE may not be a good
 183 metric for cross-study comparisons in this meta-analysis.

184

185 Table 1. Article search: '[A1 OR A2 OR A3...] AND [B1 OR B2 OR B3...] AND [C1 OR C2 OR C3 OR C4...]'

ID	A	B	C
1	Water flux	Eddy covariance	Machine learning
2	Evapotranspiration	Flux tower	Support Vector
3	Latent heat	Flux site	Neural Network
4			Random Forest

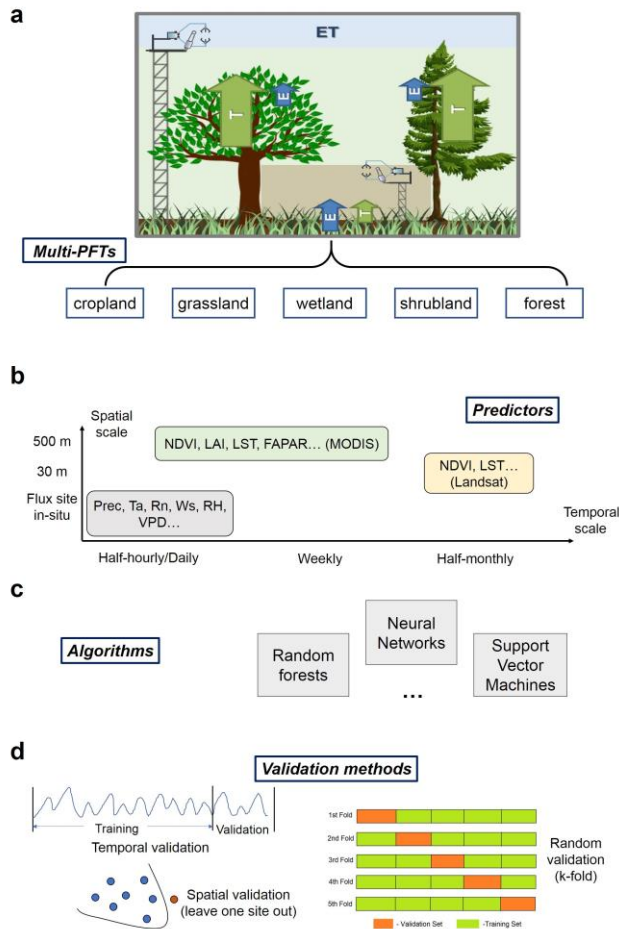
186

187 **2.2 Features of the prediction processes evaluated**

188 The various features (Table 2) involved in the water flux modeling framework (Fig. 1) include the PFTs of the
 189 sites, the predictors used, the machine learning algorithms, the validation methods, and other features. Each
 190 model for which R-squared is reported is treated as a data record. If multiple algorithms were applied to the
 191 same dataset, then multiple records were extracted. Models using different data or features are also recorded as
 192 multiple records.

设置了格式: 字体: 10 磅, 加粗

带格式的: 标题 2, 行距: 单倍行距



193
 194 Figure 1. Features of the machine learning-based water flux prediction process. (a) the eddy-covariance-based
 195 water flux observations of various plant function types (PFTs), modified from Paul-Limoges et al., 2020. ET,
 196 evapotranspiration. E, evaporation. T, transpiration. (b) Predictors and their spatial and temporal resolution. (c)
 197 The machine learning algorithms used for the modeling, such as neural networks, random forests, etc. (d) The
 198 model validation methods used including the spatial, temporal, and random cross-validations.
 199
 200

Table 2. Description of information extracted from the included papers.

Field/Feature	Definition & Categories adopted	Categories adopted Harmonization
Climate	Climate zone zones of the study location derived from the Köppen climate classification (Peel et al., 2007)	
Plant functional type (PFT)	PFT of the flux sites: 1-forest, 2-grassland, 3-cropland, 4-wetland, 5-shrubland, 6-savannah, and multi-PFTs	1-forest, 2-grassland, 3-cropland, 4-wetland, 5-shrubland, 6-savannah, and multi-PFTs The categorization is based on

带格式的: 行距: 单倍行距

带格式表格

带格式的: 行距: 单倍行距

带格式的: 行距: 单倍行距

		the descriptions in the article. For example, cropland for various crops is classified as 'cropland', and both woody savannah and savannah are classified as 'savannah'.
Location	More precise location (with the latitude and longitude of the center of the studied sites)->: <u>latitude, longitude</u>	<u>latitude, longitude</u>
Algorithms	<u>Random Forests (RF), Multiple Linear Regressions (MLR), Artificial Neural Networks (ANN), Support Vector Machines (SVM), Cubist, model tree ensembles (MTE), K-nearest neighbors (KNN), long short-term memory (LSTM), gradient boosting regression tree (GBRT), extra tree regressor (ETR), Gaussian process regression (GPR), Bayesian model averaging (BMA), extreme learning machine (ELM), and deep belief network (DBN).</u> Algorithm families used	<u>Various model algorithms with parameter optimization or other improvements are categorized as their algorithm family. For example, various improved models of RF algorithms are classified as RF, rather than as another algorithm family.</u> Random Forests (RF), Multiple Linear Regressions (MLR), Artificial Neural Networks (ANN), Support Vector Machines (SVM), Cubist, model tree ensembles (MTE), K-nearest neighbors (KNN), long short-term memory (LSTM), gradient boosting regression tree (GBRT), extra tree regressor (ETR), Gaussian process regression (GPR), Bayesian model averaging (BMA), extreme learning machine (ELM), and deep belief network (DBN)
Sites number	Number of the flux sites used	
Spatial scale	Area representatively covered by the flux sites: <u>local (less than 100 x 100 km), regional, global (continent-scale and global scale)</u>	<u>local (less than 100 x 100 km), regional, global (continent-scale and global scale)</u> The spatial scale is roughly categorized based on the area covered by the site. The model is classified as 'global' only when the spatial extent reaches the continental scale.
Temporal scale	The temporal scale of the model: <u>half-hourly, hourly, daily, 4-daily, 8-daily, monthly, seasonally (i.e., 0.02, 0.04, 1, 4, 8, 30, 90 days)</u>	<u>half-hourly, hourly, daily, 4-daily, 8-daily, monthly, seasonally (i.e., 0.02, 0.04, 1, 4, 8, 30, 90 days)</u> Models with a temporal scale greater than one month and less than one year are classified as seasonal scale models.
Year span	The span of years of the flux data used	<u>Year span is calculated as the span from the earliest to the latest year of available flux data.</u>
Site year	Describe the volume of total flux data with the number of sites and years aggregated.	
Cross-validation	Describe the chosen method of cross-validation: <u>Spatial (e.g., 'leave one site out'), temporal (e.g., 'leave one year out'), random (e.g., 'k-fold')</u>	<u>Spatial (e.g., 'leave one site out'), temporal (e.g., 'leave one year out'), random (e.g., 'k-fold')</u>
Training/validation	Describe the ratio of the data volume in the training and validation sets.	<u>In spatial validation, this ratio is represented by the ratio of the number of sites used for training to the number of sites used for validation. In temporal validation, this is represented by the ratio of the span of time periods used for</u>

带格式的: 行距: 单倍行距

带格式的: 行距: 单倍行距

带格式的: 行距: 单倍行距

带格式的: 行距: 单倍行距

带格式的: 行距: 单倍行距

带格式的: 行距: 单倍行距

带格式的: 行距: 单倍行距

带格式的: 行距: 单倍行距

带格式的: 行距: 单倍行距

带格式的: 行距: 单倍行距

		training to the span of time periods used for validation.
Satellite images	Describe the source of satellite images used to derive NDVI, EVI, LAI, LST, etc.:- Landsat, MODIS, AVHRR	Landsat, MODIS, AVHRR
Biophysical predictors	LAI, NDVI/EVI, enhanced vegetation index (EVI), the fraction of absorbed photosynthetically active radiation/photosynthetically active radiation (FAPAR/PAR), leaf area index (LAI), Carbon fluxes (CF) including NEE/GPP, etc.	Used (recorded as '1') or not used (recorded as '0')The predictor variables of different measurement methods are categorized according to their definitions. For example, both using the NDVI calculated based on satellite remote sensing bands and in situ measurements were classified as the use of 'NDVI'.
Meteorological variables	precipitation (Prec), net radiation/solar radiation (Rn/Rs), air temperature (Ta), vapour-pressure deficit (VPD), relative humidity (RH) , etc.	Used (recorded as '1') or not used (recorded as '0')The way meteorological data are measured is not differentiated. For example, both using Ta from reanalysis data and Ta measured at flux sites were classified as the use of Ta.
Ancillary data	Describe the ancillary variables used: soil texture, terrain (DEM), soil moisture/land surface water index (SM/LSWI), etc.	Used (recorded as '1') or not used (recorded as '0')Both the use of in situ measured soil moisture and the use of remote sensing-based LSWI was classified as using surface moisture-related indicators SM/LSWI.
Top three variables in the ranking of importance of predictors	Describe the interpretation of the importance of variables reported in the machine learning models.	
Accuracy measure	Accuracy measure used to assess the model performance: R-squared (in the validation phase)	R-squared (in the validation phase)

带格式的：行距：单倍行距

带格式的：行距：单倍行距

带格式的：行距：单倍行距

带格式的：行距：单倍行距

带格式的：行距：单倍行距

带格式表格

201

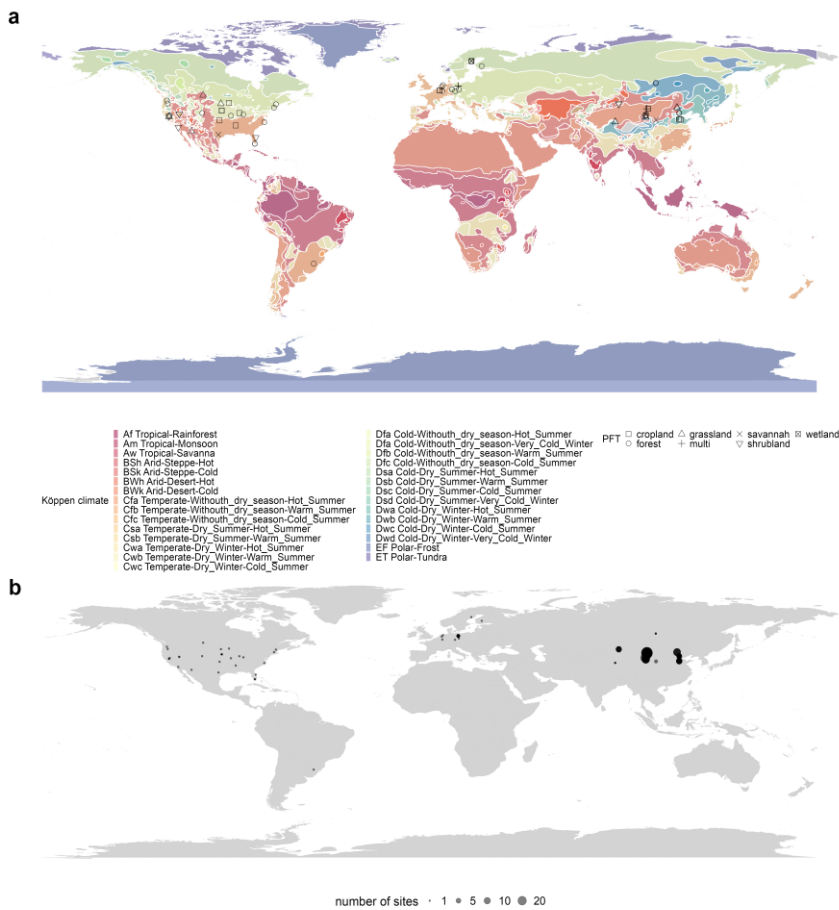
202 3 Results

203 3.1 Articles included in the meta-analysis

204 A total of 32 articles (see Supplement Information Table S1) containing a total of 139 model records were
205 included. The geographical scope of these articles was mainly Europe, North America, and China (Fig. 2).

设置了格式：字体：10 磅，加粗

带格式的：标题 2，行距：单倍行距



206
 207 Figure 2. Location of the included studies in the meta-analysis. (a) PFTs and the climate zones (from Köppen
 208 climate classification) of these studies and (b) the number of flux sites included in each study. Global and
 209 continental-scale studies (e.g., models developed based on FLUXNET of the global scale) are not shown on the
 210 map due to the difficulty of identifying specific locations.

211 **3.2 The formal Meta-analysis**

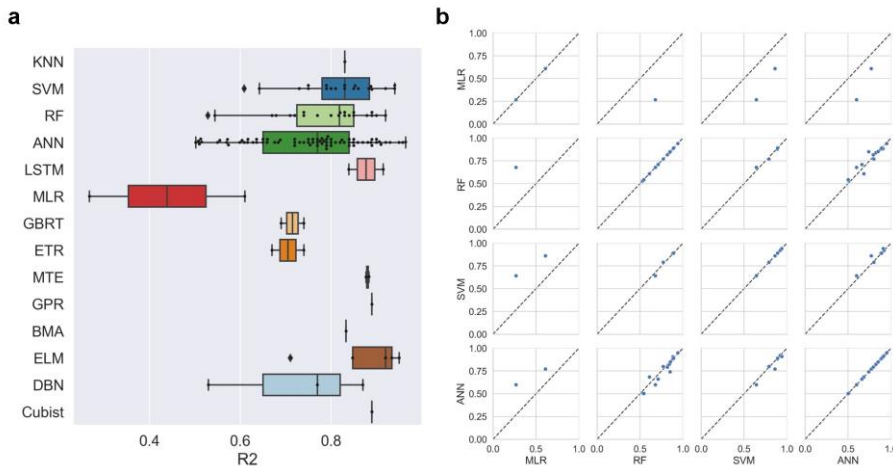
212 *We formally assessed the impact of the features (e.g., algorithms, study area, PFTs, the volume of data used,
 213 validation methods, predictor variables, etc.) used in the different models based on differences of R-squared.*

215 **3.2.1 Algorithms**

216 SVM and RF outperformed (Fig. 3a) across studies (*highly*-better than *other algorithms with sufficient sample
 217 size in Fig. 3a such as ANN*). These three machine learning algorithms (i.e., ANN, SVM, RF) were significantly
 218 more accurate than the traditional MLR. Other algorithms such as MTE, ELM, Cubist, etc. also correspond to

设置了格式: 字体: 10 磅, 加粗
 带格式的: 标题 2, 行距: 单倍行距

219 high accuracy, but with limited evidence sample size- (Fig. 3a). In the internal comparison (different algorithms
 220 applied to the same data set) in single studies, we also find that SVM and RF were significantly slightly more
 221 accurate than ANN (Fig. 3b), and all these three (i.e., ANN, SVM, RF) are significantly considerably more
 222 accurate than MLR. Overall, SVM and RF have shown higher accuracy in water flux simulations- in both inter
 223 and intra-study comparisons with sufficient sample size as evidence.

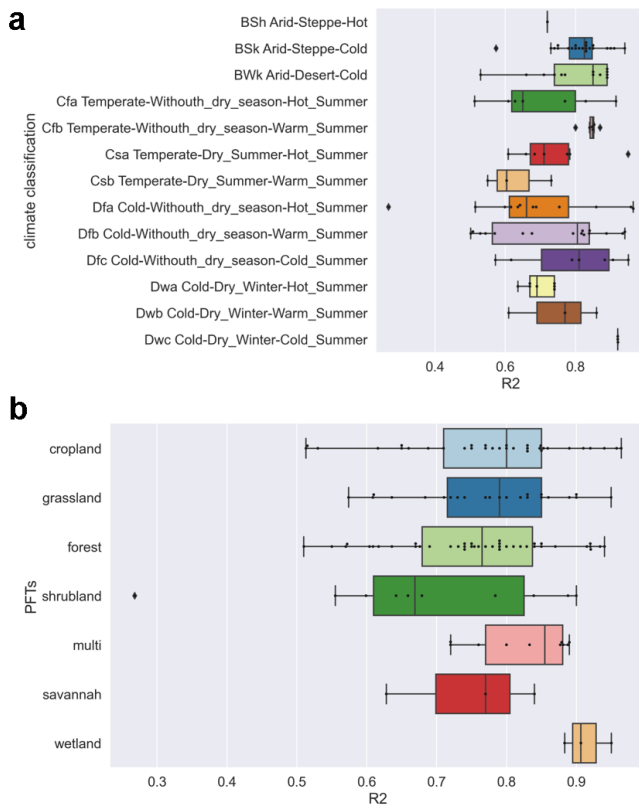


224
 225 Figure 3. Differences in model accuracy (R-squared) using different various algorithms across studies (a)
 226 and internal comparisons of the model accuracy (R-squared) of selected pairs of algorithms within individual
 227 studies (b). Regression algorithms: Algorithms: Random Forests (RF), Multiple Linear Regressions (MLR),
 228 Artificial Neural Networks (ANN), Support Vector Machines (SVM), Bayesian model averaging (BMA),
 229 Cubist, model tree ensembles (MTE), K-nearest neighbors (KNN), long short term memory (LSTM), gradient
 230 boosting regression tree (GBRT), extra tree regressor (ETR), K-nearest neighbors (KNN), long short-term
 231 memory (LSTM), Gaussian process regression (GPR), Bayesian model averaging (BMA), extreme learning
 232 machine (ELM), and deep belief network (DBN).
 233

234 3.2.2 Climate types and PFTs

235 We found higher average model accuracy in arid climate zones (Fig. 4a), such as the Cold semi-arid (steppe)
 236 climate (BSk) and Cold desert climate (BWk-). Most of these studies were located in northwest China and the
 237 western USA. It may be caused by the simpler relationship between water fluxes and biophysical covariates in
 238 arid regions. In arid zones, due to the high potential ET, the variability in the actual ET may be largely explained
 239 by water availability (moisture supply) and vegetation change with the effect of variability in thermal conditions
 240 reduced. As for the various PFTs, the average model accuracy was slightly lower for forest types than for
 241 cropland and grassland types (Fig. 4b) possibly because some remote sensing based predictors such as FAPAR
 242 and LAI have limited accuracy when applied to forest types (Fig. 5). The lowest average accuracy was found for
 243 shrub sites, which may be related to the difficulty of remote sensing based NDVI, etc., to quantify the
 244 physiological and ecological conditions of shrubs (4b). The lowest average accuracy was found for shrub sites,

245 which may be related to the difficulty of the remote sensing-based vegetation index (e.g., NDVI) to quantify the
 246 physiological and ecological conditions of shrubs (Zeng et al., 2022), and the heterogeneity of the spatial
 247 distribution of shrubs within the EC observation area may also cause difficulties in capturing their relationships
 248 with biophysical variables. We also found high model accuracy for the wetland type, although records as
 249 evidence to support this finding may be limited. Compared to other PFTs, the more steady and adequate water
 250 availability in the wetland type may make the variations of water fluxes less explained by other biophysical
 251 covariates.

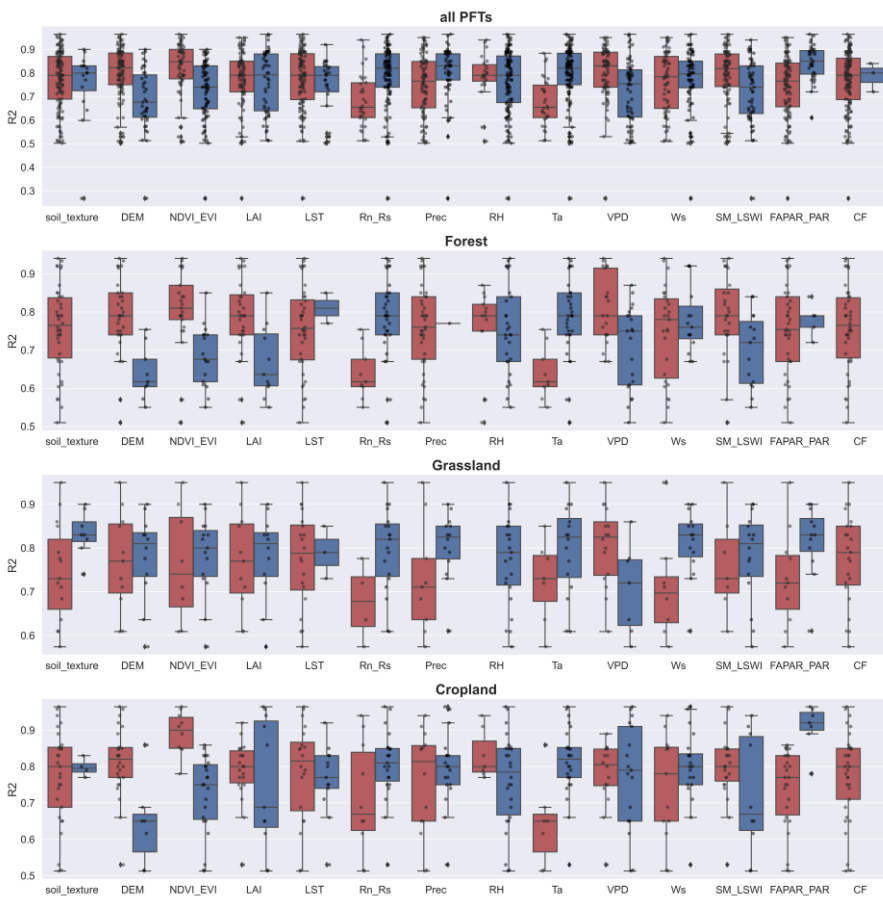


252
 253 Figure 4. Differences in model accuracy (R-squared) of (a) various climate zones (classified by Köppen climate
 254 classification) across studies and (b) PFTs. BSh, Hot semi-arid (steppe) climate. BSk, Cold semi-arid (steppe)
 255 climate. BWk, Cold desert climate. Cfa, Humid subtropical climate. Cfb, Temperate oceanic climate. Csa, Hot-
 256 summer Mediterranean climate. Csb, Warm-summer Mediterranean climate. Dfa, Hot-summer humid
 257 continental climate. Dfb, Warm-summer humid continental climate. Dfc, Subarctic climate. Dwa, Monsoon-
 258 influenced hot-summer humid continental climate. Dwb, Monsoon-influenced warm-summer humid continental
 259 climate. Dwc, Monsoon-influenced subarctic climate.

260

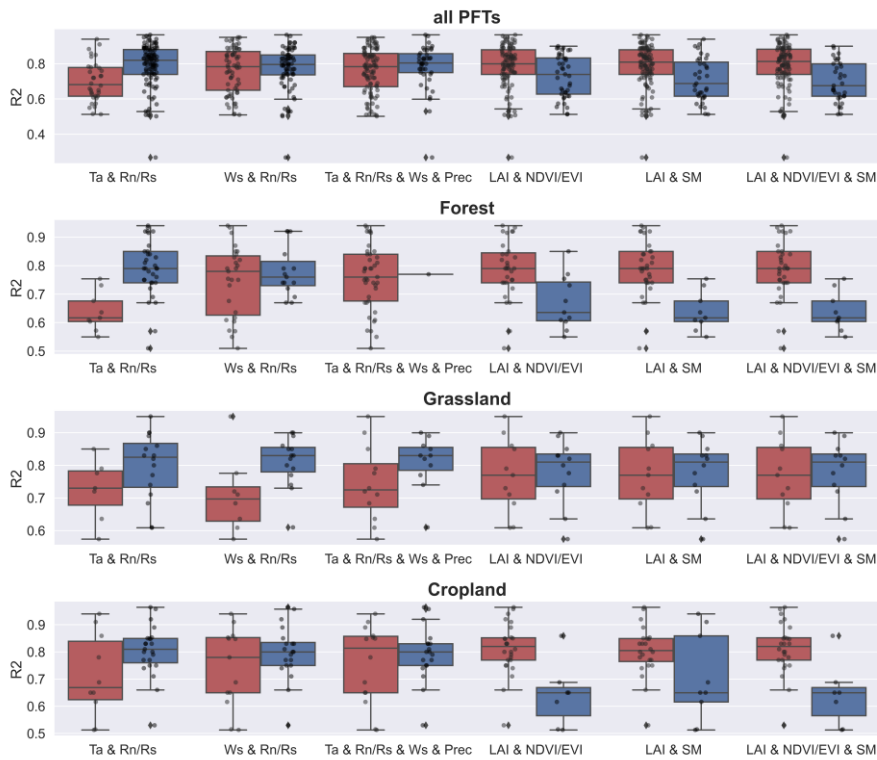
261 **Among 3.3.3 Predictors and their combinations**
 262 **On one hand, for the various effects of individual** predictors, the use of Rn/Rs, Prec, Ta, and FAPAR
 263 **significantly** improved the accuracy of the model (Fig. 5S1). This pattern partially changed in the different
 264 PFTs. In the forest sites, the accuracy of the models with Rn/Rs and Ta used was **significantly** higher than that
 265 of the models with Rn/Rs and Ta not used. For the grassland sites, the use of Ws, FAPAR, Prec, and Rn/Rs
 266 **significantly** improved the model accuracy. For the cropland sites, Ta and FAPAR were more important for
 267 improving the model accuracy.
 268

← 带格式的: 左



269
 270 **Figure 5. The impact of the various predictors used in models of different PFTs (all data, forest, grassland, and**
 271 **cropland) on R-squared. Dark blue boxes indicate that the predictor was used in the model, while dark red boxes**
 272 **indicate that the predictor was not used. Predictors: precipitation (Prec), soil moisture/land surface water index**
 273 **(SM_LSWI), net radiation/solar radiation (Rn_Rs), enhanced vegetation index (EVI), air temperature (Ta),**
 274 **vapor pressure deficit (VPD), the fraction of absorbed photosynthetically active radiation/photosynthetically**
 275 **active radiation (FAPAR_PAR), relative humidity (RH), carbon flux (CF), leaf area index (LAI).**

276
277 On the other hand, the evaluation of the effect of individual predictors on model accuracy is not necessarily
278 reliable because some predictor variables are used together (e.g., the high model accuracy corresponding to a
279 particular variable may be because it is often used together with another variable that plays the dominant role in
280 improving accuracy). Therefore, we tested for independence between the use of variables and assessed the effect
281 of the combination of variables on model accuracy. We calculated the correlation matrix (Fig. S2) between the
282 use of various predictors (not used is set as 0 and used is set as 1). We found there was a dependence between
283 the use of some predictors, the use of NDVI/EVI, LAI, and SM was significantly negatively correlated with the
284 use of Rn/Rs and Ta (Fig. S2). It indicated that many of the models that used Rn/Rs and Ta did not use
285 NDVI/EVI, LAI, and SM, and the models that used NDVI/EVI, LAI, and SM also happened to not use Rn/Rs
286 and Ta. Given this dependence, we evaluated the effect of the combination of variables on the model accuracy
287 (Fig. 5). In Fig. 5, the three variable combinations on the left side are mainly meteorological variables while the
288 three variable combinations on the right side are mainly vegetation-related variables based on remote sensing
289 (e.g., NDVI, EVI, LAI, LSWI). We found that, overall, the accuracy of the models using only meteorological
290 variable combinations was higher than that of the models using only remote sensing-based vegetation-related
291 variables. It demonstrated the importance of using meteorological variables in machine learning-based ET
292 prediction (probably especially for models with small time scales such as hourly scale, and daily scale). For
293 example, in the forest type, the combination of Ta and Rn/Rs is very effective compared to using only remote
294 sensing-based vegetation index variable combinations. The combination of Ta and Rn/Rs is also effective in the
295 grassland and cropland types. The combination of Ws and Rn/Rs played an important role in the grassland type
296 for improving model accuracy. Despite this, it does not negate the positive role of remote sensing-based
297 vegetation-related variables in ET prediction. This effectiveness can be dependent on the time scale of the model
298 as well as the PFTs. In models with large time scales (monthly scale, seasonal scale) and PFTs in which ET is
299 sensitive to vegetation dynamics, remote sensing-based vegetation-related variables may also be of high
300 importance.
301

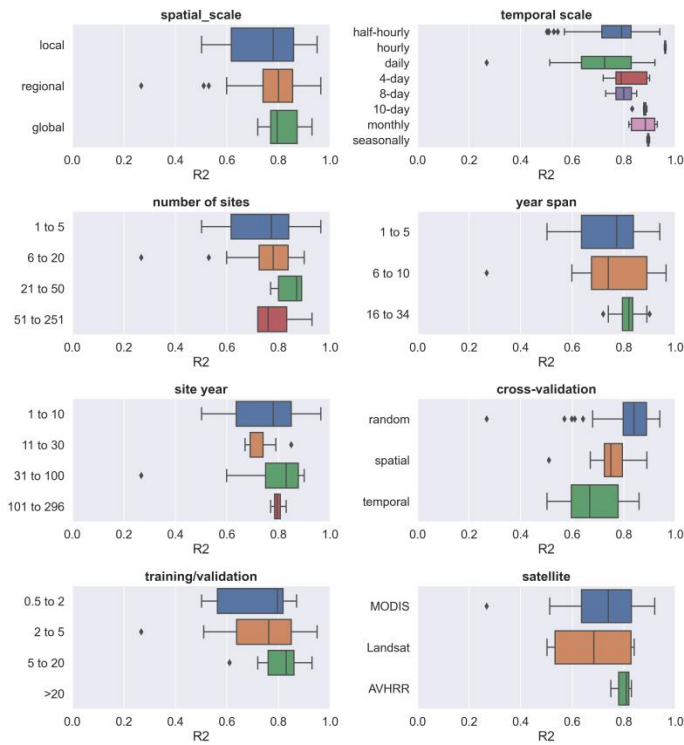


302
 303 **Figure 5.** Effects of combinations of predictor variables on model accuracy in various PFTs (all data, forest,
 304 grassland, and cropland). Dark blue boxes indicate that the predictors were together used in the model (e.g., for
 305 'Ta & Rn/Rs', the dark blue box represents Ta and Rn/Rs were together used in the model), while dark red
 306 boxes indicate the other conditions (i.e., the combination was not used). Predictors: precipitation (Prec), soil
 307 moisture/remote sensing-based land surface water index (SM), net radiation/solar radiation (Rn/Rs), enhanced
 308 vegetation index (EVI), air temperature (Ta), leaf area index (LAI), Normalized Difference Vegetation
 309 Index/Enhanced Vegetation Index (NDVI/EVI).

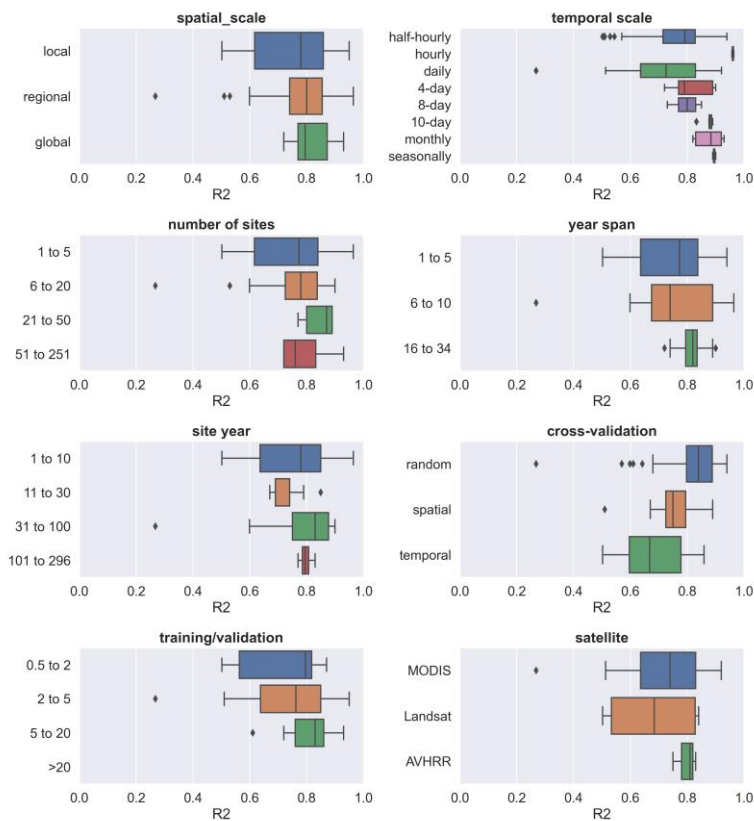
310 **3.3.4 Other model features**

311 We also evaluated the impact of some other features on accuracy. The differences in accuracy of models with
 312 different spatial scales, year spans, number of sites, and volume of data (Fig. 6) appear to be insignificant. This
 313 seems to be related to the fact that in large-scale water flux simulations, the sites of similar PFTs are selected
 314 such as for modeling multiple forest sites across Europe (Van Wijk and Bouten, 1999) which focus on 'forest'
 315 and multiple grassland sites across arid northern China (Xie et al., 2021; Zhang et al., 2021) which focus on
 316 'grassland', rather than mixing different PFT types to train models as the way in machine learning modeling of
 317 carbon fluxes (Zeng et al., 2020)(Zeng et al., 2020). In terms of the time scales of the models, the 4-day, 8-day,
 318 and monthly scales appear to correspond to higher accuracy compared to the half-hourly and daily scales. Also,

319 ~~the variability of the accuracy of the half-hourly and daily scale models is higher.~~ The higher the ratio of the
 320 volume of data in the training and validation sets, the higher the model accuracy. Compared to the models using
 321 Landsat data, the models using MODIS data showed slightly higher accuracy probably due to the advantage of
 322 MODIS data in capturing the temporal dynamics of biophysical covariates. There were significant differences in
 323 the accuracy of the models using different cross-validation methods, with the models using random cross-
 324 validation showing higher accuracy than those using temporal cross-validation. This suggests that interannual
 325 variability may have a high impact on the models in water flux simulations. The driving mechanism of ET may
 326 vary significantly across years, and the inclusion of some extreme climatic conditions in the training set may be
 327 important for model accuracy and robustness.
 328



329

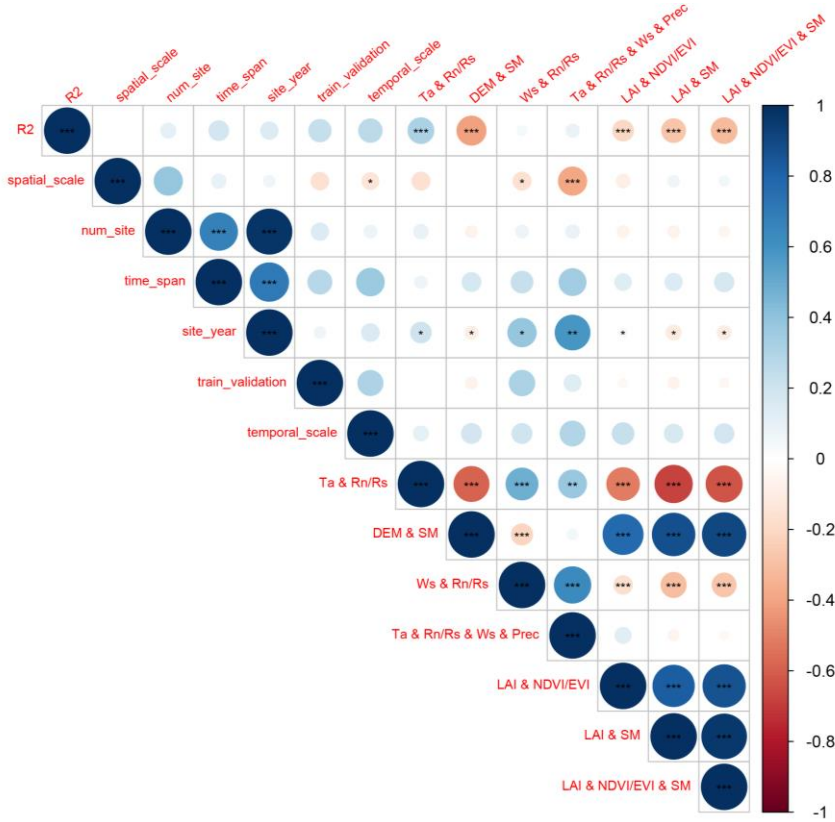


330
 331 Figure 6. The ~~impact~~ effects of other ~~model~~ features (i.e. spatial scale, ~~temporal scale~~, number of sites, ~~temporal~~
 332 ~~scale~~, year span, site year, ~~cross-validation~~ method, training/validation ~~ratio~~, and satellite imagery ~~used~~) on the
 333 ~~model performance~~. ~~R-squared~~.

334 **3.3.5 Linear correlation of quantitative features and R-squared**

335 We also analyzed the linear correlation (Fig. 7) between multiple quantitative features and the R-squared. We
 336 found that the magnitude of the linear correlation coefficients between the use of predictor combinations and the
 337 R-squared was higher than other features. The use of the predictor combination ‘Ta and Rn/Rs’ significantly
 338 improved the model accuracy. ‘Temporal scale’, ‘time span’, ‘training/validation ratio’, and ‘number of sites’
 339 showed weak positive correlations with R-squared (not significant, p-value > 0.1). The positive correlation
 340 between ‘temporal scale’ and R-squared is higher among these features, although not significant. It should also
 341 be paid more attention to in future studies. The feature ‘training/validation ratio’ and ‘time span’ are also
 342 positively correlated (although not significantly) with the R-squared, suggesting the importance of the volume of
 343 data in the training set in a data-driven machine learning model. Larger ‘training/validation ratio’ and ‘time span’
 344 may correspond to greater proportional coverage of the scenarios/conditions in the training set over the
 345 validation set, and thus correspond to higher accuracy.

346



347

348 Figure 7. Evaluation of linear correlations between multiple features and the R-squared records with the
 349 statistical significance test. For the feature ‘spatial scale’, the ‘local’ scale was set to 1, the ‘regional’ scale was
 350 set to 2, and the ‘global’ scale was set to 3 in the analysis of linear correlation. For the use of various predictor
 351 combinations with ‘&’, the value for ‘together used’ is set as 1 and other conditions are set as 0 (e.g., for the
 352 feature ‘Ta & Rn/Rs & Ws & Prec’, if Ta, Rn/Rs, Ws, and Prec were used together in the model, the value is set
 353 as 1). Significance: the p-value < 0.01 (***), 0.05 (**), and 0.1 (*).

354 **4 Discussions**

355 With the accumulation of in situ EC observations around the world, ~~compared to remote sensing or process~~
 356 ~~model-based approaches~~, the study of ET simulations based on data-driven approaches has received more
 357 attention from researchers in the last decade. Many studies have combined EC observations, various predictors,
 358 and machine learning algorithms to improve the prediction accuracy of site-scale water fluxes. To date, the
 359 results of these studies have not been comprehensively evaluated to provide clear guidance for feature selection
 360 in water flux prediction models. To better understand the approach and guide future research, we performed a

361 meta-analysis of such studies. Machine learning-based water flux simulations and predictions still suffer from
362 high uncertainty. By investigating the expected improvements that can be achieved by incorporating different
363 features, we can avoid practices that may reduce model accuracy in future research.

364 **4.1 Opportunities and challenges in the site-scale water flux simulation**

365 In the above meta-analysis of the models, we found that water flux simulations based on EC observations can
366 achieve high accuracy but also have high uncertainty through the modeling workflow. The R-squared of many
367 water flux simulation models exceeds 0.8, possibly higher than some remote sensing-based and process-based
368 models, and possibly higher than carbon flux simulations in the same modeling framework. This suggests that in
369 general, these currently-used biophysical and meteorological variables are closely related to water fluxes, such as
370 the net ecosystem exchange (Shi et al., 2022) in the same modeling framework.

371
372 Biophysical and meteorological variables are considered both important in ET simulations. This study found
373 that models using a combination of meteorological variables had higher accuracy than models using only
374 remotely sensed vegetation dynamic information. However, due to the high proportion of models with small
375 temporal scales (e.g., half-hourly scale, hourly scale, and daily scale) in this study, this advantage of the
376 combination of meteorological variables may be more suitable for small temporal scales. A possible explanation
377 is that vegetation-related variables such as NDVI and LAI at the daily scale, 8-day scale, and 16-day scale have
378 limited explanatory ability for hourly or daily-scale variability in ET. At a small temporal scale, the use of
379 combinations of meteorological variables can capture moisture and energy conditions that control the rapid
380 fluctuations of ET and thus has a dominant role in hourly or daily-scale ET prediction. This also corroborates
381 the high accuracy of some physic-based ET estimation models (Rigden and Salvucci, 2015) that use only
382 meteorological variables and not vegetation-related variables such NDVI (only an estimate of vegetation height
383 derived from land cover maps is used to represent vegetation conditions (Rigden and Salvucci, 2015)).

384
385 There are differences in model accuracy among different PFTs. For example, in forest sites, limitations in data
386 accuracy of factors were possible because some remote sensing-based predictors such as FAPAR and LAI have
387 limited accuracy when applied to forest types (Liu et al., 2018b). NDVI, FAPAR, and LAI have limited accuracy
388 when applied to forest types (Liu et al., 2018b; Zeng et al., 2022). In addition, factors such as crown density,
389 which may significantly affect the proportion of soil evaporation, transpiration, and evaporation of canopy
390 interception, were not considered in these models, which may also lead to low model accuracy. This suggests
391 that in water flux simulation, the driving mechanisms of water fluxes in different PFTs do affect the accuracy of
392 machine learning models, and we need to consider more the actual and specific influencing factors in specific
393 PFTs. More variables that can quantify the ratio of evaporation and transpiration should be considered for
394 inclusion, which also appears to improve the mechanistic interpretability of such machine learning models.
395 Several studies A previous study (Zhao et al., 2019) have has combined the physics-based approach (e.g.,
396 Penman-Monteith equation) and machine learning to build hybrid models to improve interpretability. We should
397 make full use of empirical knowledge and experiences from process-based models to improve the accuracy and
398 interpretability of the machine learning approach.

399

设置了格式: 字体: 10 磅, 加粗

带格式的: 标题 2, 行距: 单倍行距

400 The impact of differences in different satellite images on model accuracy and performance may be limited since
401 most studies used windows of 2 km x 2 km or 3 km x 3 km when extracting covariates based on satellite remote
402 sensing (Walther et al., 2021) and the effects of differences in image resolution were smoothed out (i.e., the
403 differences in values averaged over a 2 km window may not be significant at 30m and 500m resolutions).
404 However, the coarse resolution of MODIS images may not be effective when the extraction window is smaller
405 (e.g., 200 m) to reduce the inconsistency of the flux footprint extent and the extracted covariates from remote
406 sensing images due to the non-homogeneity of the underlying conditions (Chu et al., 2021). Compared to the
407 16 daily temporal scale of Landsat data, the daily or 8 daily temporal scale of MODIS data may improve the
408 accuracy slightly possibly because more temporal dynamic information is explained. The inclusion of some
409 ancillary variables that do not have the temporal dimension (e.g., soil texture, topographic variables) may be of
410 more limited use unless the model includes many flux sites for which the spatial variability of the ancillary
411 variables is large enough and does affect water fluxes.

412
413 Among the different validation methods, random cross-validation has higher accuracy than spatial cross-
414 validation and temporal cross-validation. However, spatial cross-validation and temporal cross-validation may
415 be able to better help us recognize the robustness of the model when extrapolated (i.e., applied to new stations
416 and new years). The lower accuracy in the temporal cross-validation approach implies that we need to focus on
417 interannual hydrological and meteorological variability in the water flux simulations. In cropland sites, we may
418 also need to pay more attention to the effects of interannual variability in anthropogenic cropping patterns. If
419 some extreme weather years are not included, the robustness of the model when extrapolated to other years may
420 be challenged, especially in the context of the various extreme weather events of recent years. This can also
421 inform the siting of future flux stations. Regions where climate extremes may occur and biogeographic types not
422 covered by existing flux observation networks should be given more attention to achieve global-scale, accurate
423 and robust machine learning-based spatio-temporal prediction of water fluxes.

424 **4.2 Uncertainties and limitations of this meta-analysis**

425 **4.2.1 The potential uncertainties and limitations of the results of this meta-analysis are as follows:**

426 **The limited number of available literature and model records that can be collected:**

427 a) Despite many articles and model records collected through our efforts to perform this meta-analysis,
428 there still appears to be a long way to go to finally and completely understand the various mechanisms involved
429 in water flux simulation with machine learning. Some of the insights provided by this study can be not robust
430 (due to the limited sample size available when the goal is to assess the effects of multiple features), but this does
431 not negate the fact that this study does obtain some meaningful findings. Therefore, researchers should treat the
432 results of this study with caution, as they were obtained only statistically. Overall, it is still positive to conduct a
433 meta-analysis of such studies, considering their rapid growth in the number and lack of guiding directions.

434 **4.2.2 Publication bias and weighting**

435 b) Publication bias and weighting: Due to the relatively limited number of articles that could be included
436 in the meta-analysis, this study did not focus much on publication bias. Meta-analytic studies in other fields

设置了格式: 字体: 10 磅, 加粗

带格式的: 标题 2, 行距: 单倍行距

设置了格式: 字体: 加粗

设置了格式: 字体: 加粗

带格式的: 正文, 无项目符号或编号

带格式的: 正文, 无项目符号或编号

437 typically measure the quality of journals and the public availability of research data (Borenstein et al., 2011;
438 Field and Gillett, 2010) to determine the weighting ~~in~~of the literature in a comprehensive assessment. However,
439 most of the articles did not publicly provide flux observations or share developed models. Meta-analysis studies
440 in other fields typically measure the impact of included studies based on sample size and variance of
441 experimental results (Adams et al., 1997; Don et al., 2011; Liu et al., 2018a). In this study, due to the lack of a
442 convincing manner to determine weights among articles, we assigned the same weight to the results for all the
443 literature.

444 **4.2.3 Uncertainties in the information of the extracted features:** ~~First, as most studies used far more water~~
445 ~~flux observation records than~~

446 ~~At the number of covariates in their regression models, we did not adjust information extraction level, the R-~~
447 ~~squared in this study to an adjusted R-squared. Secondly, following issues may also introduce uncertainties:~~

448 a) ~~Uncertainties~~ caused by data quality control (e.g. gap-filling (Hui et al., 2004)) ~~and differences in the eddy~~
449 ~~covariance observation instruments used to observe water fluxes, etc., are difficult to assess effectively.~~

450 ~~Thirdly, there~~ are difficult to assess effectively. Gap-filling is a commonly used technique to fill in low-
451 ~~quality data in flux observations (Chen et al., 2012; Hui et al., 2004). However, the impact of this practice~~
452 ~~on machine learning-based ET prediction models is unclear, due to the difficulty of directly assessing how~~
453 ~~this technique is performed in various studies by this meta-analysis. Typically, models with small time~~
454 ~~scales (e.g., hourly scale, daily scale) can exclude low-quality observations and use only high-quality data.~~
455 ~~However, for models with large time scales (e.g., monthly scales), gap-filling (e.g., based on~~
456 ~~meteorological data) may be unavoidable. This may lead to decrease in training data purity and introduce~~
457 ~~uncertainty in the subsequent prediction model development.~~

458 b) ~~Systematic uncertainties caused by the energy balance closure (EBC) issue in eddy-covariance flux~~
459 ~~measurements are also difficult to assess by this meta-analysis. EBC is a common problem (Eshonkulov et~~
460 ~~al., 2019) in eddy-covariance flux observations. For that reason, the latent heat flux measured potentially~~
461 ~~underestimates ET. Some prediction models corrected EBC (e.g., using Bowen ratio preserving (Mauder et~~
462 ~~al., 2013, 2018) and energy balance residuals (Charuchittipan et al., 2014; Mauder et al., 2018)) in the~~
463 ~~processing of training data, but some did not. How this will affect the accuracy of the prediction model is~~
464 ~~not clear due to multiple factors that need to be evaluated that influence EBC (Foken, 2008), including~~
465 ~~measurement errors of the energy balance components, incorrect sensor configurations, influences of~~
466 ~~heterogeneous canopy height, unconsidered energy storage terms in the soil-plant-atmosphere system,~~
467 ~~inadequate time averaging intervals, and long-wave eddies (Jacobs et al., 2008; Foken, 2008; Eshonkulov~~
468 ~~et al., 2019). To reduce this uncertainty, more attention to flux site characteristics (Eshonkulov et al., 2019)~~
469 ~~related to PFT, topography, flux footprint area, etc., to select the appropriate correction method is~~
470 ~~necessary for future studies.~~

471 c) ~~As most studies used far more water flux observation records than the number of covariates in their~~
472 ~~regression models, we did not adjust the R-squared in this study to an adjusted R-squared.~~

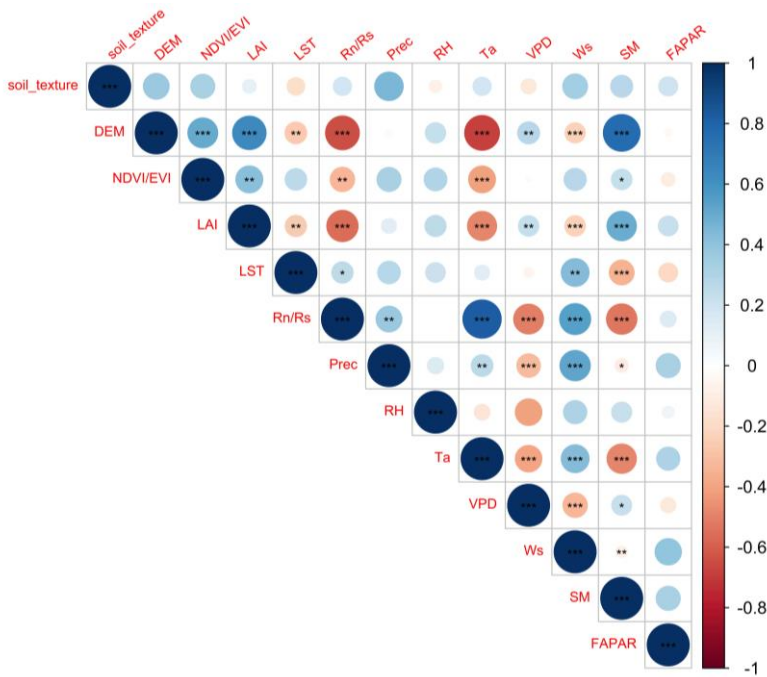
473 d) ~~The~~ various specific ways in which the parameters of the model are optimized are not differentiated. They
474 are broadly categorized into different families or kinds of algorithms, which may also introduce uncertainty
475 into the assessment. ~~Fourth, the~~

设置了格式: 字体: 加粗

476 e)e) The assessment of some features is not detailed due to the limitations of the available model records. For
 477 example, the classification of PFT could be more detailed. 'Forest' could be further classified as broadleaf
 478 forest, coniferous forest, etc. while 'cropland' could be further classified as rainfed and irrigated cropland
 479 based on differences in their response mechanisms of water fluxes to environmental factors.

480 d) Independence between features: There is dependence between some of the features being evaluated, which
 481 may affect the assessment of the impact of single features on the accuracy of the model. We found that the
 482 use of NDVI/EVI, LAI, VPD, and SM was significantly negatively correlated with the use of Rn/Rs and Ta
 483 (Fig. 7) when unused was set to 0 and used was set to 1. It means that many of the models that used Rn/Rs
 484 and Ta did not use NDVI/EVI, LAI, VPD, and SM, and the models that used NDVI/EVI, LAI, VPD, and
 485 SM also happened to not use Rn/Rs and Ta. It can indirectly explain the fact that the accuracy of the models
 486 with NDVI/EVI, LAI, VPD, and SM is even lower than that of the models without NDVI/EVI, LAI, VPD,
 487 and SM in the above analysis (Fig. 5) because of the disturbance from the use of Rn/Rs and Ta.

带格式的: 编号 + 级别: 1 + 编号样式: a, b, c, ...
 + 起始编号: 1 + 对齐方式: 左侧 + 对齐位置: 0 厘米
 + 缩进位置: 0.74 厘米



488 Fig. 7. Correlation matrix between the use of various predictors (not used is set as 0 and used is set as 1) which
 489 may introduce uncertainty in the assessment of the impact of an individual predictor on model performance.
 490 Significance: the p-value < 0.01 (***), 0.05 (**), and 0.1 (*).
 491

492 **5 Conclusion**

493 We performed a meta-analysis of the site-scale water flux simulations combining in situ flux observations,
494 meteorological, biophysical, and ancillary predictors, and machine learning. The main conclusions are as
495 follows:

- 496 a)1. SVM (average R-squared = 0.82) and RF (average R-squared = 0.81) outperformed over evaluated
497 algorithms with sufficient sample size in both cross-study and intra-study (with the same training dataset)
498 comparisons.
- 499 b)2. The average accuracy of the model applied to arid regions is higher than in other climate ~~classes~~types.
- 500 e)3. The average accuracy of the model was slightly lower for forest sites (average R-squared = 0.76) than for
501 cropland and grassland sites (average R-squared = 0.8 and 0.79), but higher than for shrub sites (average R-
502 squared = 0.67).
- 503 d)4. Among various predictor variables, the use of Rn/Rs, Prec, Ta, and FAPAR improved the model accuracy.
504 The combination of Ta and Rn/Rs is very effective especially in the forest type, while in the grassland type
505 the combination of Ws and Rn/Rs is also effective.
- 506 e)5. Among the different validation methods, random cross-validation shows higher model accuracy than spatial
507 cross-validation and temporal cross-validation.

508
509
510

带格式的: 多级符号 + 级别: 1 + 编号样式: 1, 2, 3, ... + 起始编号: 1 + 对齐方式: 左侧 + 对齐位置: 0 厘米 + 缩进位置: 0.63 厘米

511 **Acknowledgements**

512 We thank the editor and two anonymous reviewers for their insightful comments which contributed substantially
513 to the improvement of this manuscript.

514 **Financial support**

515 This research was supported by the National Natural Science Foundation of China (Grant No. U1803243), the
516 Key projects of the Natural Science Foundation of Xinjiang Autonomous Region (Grant No. 2022D01D01), the
517 Strategic Priority Research Program of the Chinese Academy of Sciences (Grant No. XDA20060302), and High-
518 End Foreign Experts Project.

519 **Author Contributions**

520 ~~Haiyang Shi: Conceptualization, Methodology, Data, Writing. Geping Luo: Conceptualization, Supervision,~~
521 ~~Revision. Olaf Hellwich: Methodology. Alishir Kurban: Supervision. Tim Van De Voorde: Supervision. Philippe~~
522 ~~De Maeyer: Supervision, Revision. Xiaofei Ma, Xiuliang Yuan, Yuangang Wang, Wenqiang Zhang, Mingjuan~~
523 ~~Xie, Chen Zhang, Yu Zhang: Data.~~

524 HS and GL were responsible for the conceptualization, methodology, formal analysis, investigation, visualization,
525 and writing. OH contributed to the investigation. XM, XY, YW, WZ, MX, CZ and YZ processed the data. AK,
526 TVDV and PDM provided supervision.

527 **Competing interests**

528 The authors declare that they have no conflict of interest.

529 **Code availability**

530 The codes that were used for all analyses are available from the first author (shihaiyang16@mails.ucas.ac.cn)
531 upon request.

532 **Data availability**

533 The data used in this study can be accessed by contacting the first author (shihaiyang16@mails.ucas.ac.cn)
534 ~~based on reasonable~~upon request.

535

设置了格式: 字体: 宋体

536 **References**

- 537 [Adams, D. C., Gurevitch, J., and Rosenberg, M. S.: Resampling tests for meta - analysis of ecological](#)
538 [data, Ecology, 78, 1277–1283, 1997.](#)
- 539 [Allen, R. G., Pereira, L. S., Howell, T. A., and Jensen, M. E.: Evapotranspiration information](#)
540 [reporting: I. Factors governing measurement accuracy, Agricultural Water Management, 98, 899–920,](#)
541 <https://doi.org/10.1016/j.agwat.2010.12.015>, 2011.
- 542 [Anderson, M. C., Allen, R. G., Morse, A., and Kustas, W. P.: Use of Landsat thermal imagery in](#)
543 [monitoring evapotranspiration and managing water resources, Remote Sensing of Environment, 122,](#)
544 [50–65, https://doi.org/10.1016/j.rse.2011.08.025](https://doi.org/10.1016/j.rse.2011.08.025), 2012.
- 545 [Barman, R., Jain, A. K., and Liang, M.: Climate-driven uncertainties in modeling terrestrial energy](#)
546 [and water fluxes: a site-level to global-scale analysis, 20, 1885–1900,](#)
547 <https://doi.org/10.1111/gcb.12473>, 2014.
- 548 [Borenstein, M., Hedges, L. V., Higgins, J. P., and Rothstein, H. R.: Introduction to meta-analysis,](#)
549 [John Wiley & Sons, 2011.](#)
- 550 [Charuchittipan, D., Babel, W., Mauder, M., Leps, J.-P., and Foken, T.: Extension of the Averaging](#)
551 [Time in Eddy-Covariance Measurements and Its Effect on the Energy Balance Closure, Boundary-](#)
552 [Layer Meteorol, 152, 303–327, https://doi.org/10.1007/s10546-014-9922-6, 2014.](#)
- 553 [Chen, Y., Xia, J., Liang, S., Feng, J., Fisher, J. B., Li, X., Li, X., Liu, S., Ma, Z., Miyata, A., Mu, Q.,](#)
554 [Sun, L., Tang, J., Wang, K., Wen, J., Xue, Y., Yu, G., Zha, T., Zhang, L., Zhang, Q., Zhao, T., Zhao,](#)
555 [L., and Yuan, W.: Comparison of satellite-based evapotranspiration models over terrestrial](#)
556 [ecosystems in China, Remote Sensing of Environment, 140, 279–293,](#)
557 <https://doi.org/10.1016/j.rse.2013.08.045>, 2014.
- 558 [Chen, Y., Wang, S., Ren, Z., Huang, J., Wang, X., Liu, S., Deng, H., and Lin, W.: Increased](#)
559 [evapotranspiration from land cover changes intensified water crisis in an arid river basin in northwest](#)
560 [China, Journal of Hydrology, 574, 383–397, https://doi.org/10.1016/j.jhydrol.2019.04.045, 2019.](#)
- 561 [Chu, H., Luo, X., Ouyang, Z., Chan, W. S., Dengel, S., Biraud, S. C., Torn, M. S., Metzger, S., Kumar, J.,](#)
562 [Arain, M. A., Arkebauer, T. J., Baldochi, D., Bernacchi, C., Billesbach, D., Black, T. A., Blanken, P. D.,](#)
563 [Bohrer, G., Bracho, R., Brown, S., Brunzell, N. A., Chen, J., Chen, X., Clark, K., Desai, A. R., Duman, T.,](#)
564 [Durden, D., Fares, S., Forbrich, I., Gamon, J. A., Gough, C. M., Griffis, T., Helbig, M., Hollinger, D.,](#)
565 [Humphreys, E., Ikawa, H., Iwata, H., Ju, Y., Knowles, J. F., Knox, S. H., Kobayashi, H., Kolb, T., Law, B., Lee,](#)
566 [X., Litvak, M., Liu, H., Munger, J. W., Noormets, A., Novick, K., Oberbauer, S. F., Oechel, W., Oikawa, P.,](#)
567 [Papuga, S. A., Pendall, E., Prajapati, P., Prueger, J., Quinton, W. L., Richardson, A. D., Russell, E. S., Scott, R.](#)
568 [L., Starr, G., Staebler, R., Stoy, P. C., Stuart Haëntjens, E., Sonntag, O., Sullivan, R. C., Suyker, A., Ueyama,](#)
569 [M., Vargas, R., Wood, J. D., and Zona, D.: Representativeness of Eddy Covariance flux footprints for areas](#)
570 [surrounding AmeriFlux sites, Agricultural and Forest Meteorology, 301–302, 108350,](#)
571 <https://doi.org/10.1016/j.agrformet.2021.108350>, 2021.
- 572 [Chen, Y.-Y., Chu, C.-R., and Li, M.-H.: A gap-filling model for eddy covariance latent heat flux:](#)
573 [Estimating evapotranspiration of a subtropical seasonal evergreen broad-leaved forest as an example,](#)
574 [468–469, 101–110, https://doi.org/10.1016/j.jhydrol.2012.08.026](https://doi.org/10.1016/j.jhydrol.2012.08.026), 2012.
- 575 [Don, A., Schumacher, J., and Freibauer, A.: Impact of tropical land-use change on soil organic carbon](#)
576 [stocks – a meta-analysis, 17, 1658–1670, https://doi.org/10.1111/j.1365-2486.2010.02336.x, 2011.](#)
- 577 [Eshonkulov, R., Poyda, A., Ingwersen, J., Wizemann, H.-D., Weber, T. K. D., Kremer, P., Högy, P.,](#)
578 [Pulatov, A., and Streck, T.: Evaluating multi-year, multi-site data on the energy balance closure of](#)

设置了格式: 字体: 11 磅

设置了格式: 字体: 11 磅

设置了格式: 字体: 11 磅

579 [eddy-covariance flux measurements at cropland sites in southwestern Germany, 16, 521–540,](#)
580 <https://doi.org/10.5194/bg-16-521-2019>, 2019.

581 [Fang, B., Lei, H., Zhang, Y., Quan, Q., and Yang, D.: Spatio-temporal patterns of evapotranspiration](#)
582 [based on upscaling eddy covariance measurements in the dryland of the North China Plain, 281,](#)
583 <https://doi.org/10.1016/j.agrformet.2019.107844>, 2020.

584 Field, A. P. and Gillett, R.: How to do a meta - analysis, *British Journal of Mathematical and*
585 *Statistical Psychology*, 63, 665–694, 2010.

586 Fisher, J. B., Melton, F., Middleton, E., Hain, C., Anderson, M., Allen, R., McCabe, M. F., Hook, S.,
587 Baldocchi, D., Townsend, P. A., Kilic, A., Tu, K., Miralles, D. D., Perret, J., Lagouarde, J.-P.,
588 Waliser, D., Purdy, A. J., French, A., Schimel, D., Famiglietti, J. S., Stephens, G., and Wood, E. F.:
589 The future of evapotranspiration: Global requirements for ecosystem functioning, carbon and climate
590 feedbacks, agricultural management, and water resources, 53, 2618–2626,
591 <https://doi.org/10.1002/2016WR020175>, 2017.

592 [Foken, T.: The energy balance closure problem: An overview, *Ecological Applications*, 18, 1351–](#)
593 [1367, 2008.](#)

594 [Gaston, K. J.: Global patterns in biodiversity, 405, 220–227, https://doi.org/10.1038/35012228, 2000.](#)

595 Hui, D., Wan, S., Su, B., Katul, G., Monson, R., and Luo, Y.: Gap-filling missing data in eddy
596 covariance measurements using multiple imputation (MI) for annual estimations, 121, 93–111,
597 [https://doi.org/10.1016/S0168-1923\(03\)00158-8](https://doi.org/10.1016/S0168-1923(03)00158-8), 2004.

598 [Jacobs, A. F. G., Heusinkveld, B. G., and Holtslag, A. A. M.: Towards Closing the Surface Energy](#)
599 [Budget of a Mid-latitude Grassland, *Boundary-Layer Meteorol.*, 126, 125–136,](#)
600 <https://doi.org/10.1007/s10546-007-9209-2>, 2008.

601 [Jung, M., Reichstein, M., and Bondeau, A.: Towards global empirical upscaling of FLUXNET eddy](#)
602 [covariance observations: Validation of a model tree ensemble approach using a biosphere model, 6,](#)
603 <https://doi.org/10.5194/bg-6-2001-2009>, 2009.

604 Jung, M., Reichstein, M., Margolis, H. A., Cescatti, A., Richardson, A. D., Arain, M. A., Arneeth, A.,
605 Bernhofer, C., Bonal, D., Chen, J., Gianelle, D., Gobron, N., Kiely, G., Kutsch, W., Lasslop, G., Law,
606 B. E., Lindroth, A., Merbold, L., Montagnani, L., Moors, E. J., Papale, D., Sottocornola, M., Vaccari,
607 F., and Williams, C.: Global patterns of land-atmosphere fluxes of carbon dioxide, latent heat, and
608 sensible heat derived from eddy covariance, satellite, and meteorological observations, 116,
609 <https://doi.org/10.1029/2010JG001566>, 2011.

610 Kaur, H., Pannu, H. S., and Malhi, A. K.: A Systematic Review on Imbalanced Data Challenges in
611 Machine Learning: Applications and Solutions, *ACM Comput. Surv.*, 52, 79:1-79:36,
612 <https://doi.org/10.1145/3343440>, 2019.

613 Li, X., He, Y., Zeng, Z., Lian, X., Wang, X., Du, M., Jia, G., Li, Y., Ma, Y., Tang, Y., Wang, W., Wu,
614 Z., Yan, J., Yao, Y., Ciais, P., Zhang, X., Zhang, Y., Zhang, Y., Zhou, G., and Piao, S.:
615 Spatiotemporal pattern of terrestrial evapotranspiration in China during the past thirty years, 259,
616 131–140, <https://doi.org/10.1016/j.agrformet.2018.04.020>, 2018.

617 [Li, X., Kang, S., Niu, J., Huo, Z., and Liu, J.: Improving the representation of stomatal responses to](#)
618 [CO₂ within the Penman–Monteith model to better estimate evapotranspiration responses to climate](#)
619 [change, *Journal of Hydrology*, 572, 692–705, https://doi.org/10.1016/j.jhydrol.2019.03.029, 2019.](#)

设置了格式: 字体: 11 磅

设置了格式: 字体: 11 磅

设置了格式: 字体: 11 磅

620 [Liu, Q., Zhang, Y., Liu, B., Amonette, J. E., Lin, Z., Liu, G., Ambus, P., and Xie, Z.:](#) How does
621 biochar influence soil N cycle? A meta-analysis, *Plant and soil*, 426, 211–225, 2018a.

622 [Liu, Y., Xiao, J., Ju, W., Zhu, G., Wu, X., Fan, W., Li, D., and Zhou, Y.:](#) Satellite-derived LAI
623 products exhibit large discrepancies and can lead to substantial uncertainty in simulated carbon and
624 water fluxes, *Remote Sensing of Environment*, 206, 174–188,
625 <https://doi.org/10.1016/j.rse.2017.12.024>, 2018b.

626 [Lu, X. and Zhuang, Q.:](#) Evaluating evapotranspiration and water-use efficiency of terrestrial
627 ecosystems in the conterminous United States using MODIS and AmeriFlux data,
628 <https://doi.org/10.1016/j.rse.2010.04.001>, 2010.

629 [Mauder, M., Cuntz, M., Drüe, C., Graf, A., Rebmann, C., Schmid, H. P., Schmidt, M., and](#)
630 [Steinbrecher, R.:](#) A strategy for quality and uncertainty assessment of long-term eddy-covariance
631 measurements, *Agricultural and Forest Meteorology*, 169, 122–135,
632 <https://doi.org/10.1016/j.agrformet.2012.09.006>, 2013.

633 [Mauder, M., Genzel, S., Fu, J., Kiese, R., Soltani, M., Steinbrecher, R., Zeeman, M., Banerjee, T., De](#)
634 [Roo, F., and Kunstmann, H.:](#) Evaluation of energy balance closure adjustment methods by
635 independent evapotranspiration estimates from lysimeters and hydrological simulations, 32, 39–50,
636 <https://doi.org/10.1002/hyp.11397>, 2018.

637 [McColl, K. A.:](#) Practical and Theoretical Benefits of an Alternative to the Penman-Monteith
638 Evapotranspiration Equation, 56, e2020WR027106, <https://doi.org/10.1029/2020WR027106>, 2020.

639 [Minacapilli, M., Agnese, C., Blanda, F., Cammalleri, C., Ciraolo, G., D’Urso, G., Iovino, M., Pumo,](#)
640 [D., Provenzano, G., and Rallo, G.:](#) Estimation of actual evapotranspiration of Mediterranean perennial
641 crops by means of remote-sensing based surface energy balance models, 13, 1061–1074,
642 <https://doi.org/10.5194/hess-13-1061-2009>, 2009.

643 [Miralles, D. G., Holmes, T. R. H., De Jeu, R. a. M., Gash, J. H., Meesters, A. G. C. A., and Dolman,](#)
644 [A. J.:](#) Global land-surface evaporation estimated from satellite-based observations, 15, 453–469,
645 <https://doi.org/10.5194/hess-15-453-2011>, 2011.

646 [Miralles, D. G., Teuling, A. J., van Heerwaarden, C. C., and Vilà-Guerau de Arellano, J.:](#) Mega-
647 heatwave temperatures due to combined soil desiccation and atmospheric heat accumulation, *Nature*
648 *Geosci*, 7, 345–349, <https://doi.org/10.1038/ngeo2141>, 2014.

649 [Moher, D., Liberati, A., Tetzlaff, J., Altman, D. G., and Prisma Group:](#) Preferred reporting items for
650 systematic reviews and meta-analyses: the PRISMA statement, *PLoS medicine*, 6, e1000097, 2009.

651 [Mu, Q., Zhao, M., and Running, S. W.:](#) Improvements to a MODIS global terrestrial
652 evapotranspiration algorithm, *Remote Sensing of Environment*, 115, 1781–1800,
653 <https://doi.org/10.1016/j.rse.2011.02.019>, 2011.

654 [Pan, S., Tian, H., Dangal, S. R. S., Yang, Q., Yang, J., Lu, C., Tao, B., Ren, W., and Ouyang, Z.:](#)
655 Responses of global terrestrial evapotranspiration to climate change and increasing atmospheric CO₂
656 in the 21st century, 3, 15–35, <https://doi.org/10.1002/2014EF000263>, 2015.

657 [Pan, S., Pan, N., Tian, H., Friedlingstein, P., Sitch, S., Shi, H., Arora, V. K., Haverd, V., Jain, A. K.,](#)
658 [Kato, E., Lienert, S., Lombardozzi, D., Nabel, J. E. M. S., Ottlé, C., Poulter, B., Zaehle, S., and](#)
659 [Running, S. W.:](#) Evaluation of global terrestrial evapotranspiration using state-of-the-art approaches
660 in remote sensing, machine learning and land surface modeling, 24, 1485–1509,
661 <https://doi.org/10.5194/hess-24-1485-2020>, 2020.

设置了格式: 字体: 11 磅

设置了格式: 字体: 11 磅

662 Papale, D., Black, T. A., Carvalhais, N., Cescatti, A., Chen, J., Jung, M., Kiely, G., Lasslop, G.,
663 Mahecha, M. D., Margolis, H., Merbold, L., Montagnani, L., Moors, E., Olesen, Jø. E., Reichstein,
664 M., Tramontana, G., Van Gorsel, E., Wohlfahrt, G., and Ráduly, B.: Effect of spatial sampling from
665 European flux towers for estimating carbon and water fluxes with artificial neural networks, 120,
666 1941–1957, <https://doi.org/10.1002/2015JG002997>, 2015.

667 Paul-Limoges, E., Wolf, S., Schneider, F. D., Longo, M., Moorcroft, P., Gharun, M., and Damm, A.:
668 Partitioning evapotranspiration with concurrent eddy covariance measurements in a mixed forest,
669 *Agricultural and Forest Meteorology*, 280, 107786, <https://doi.org/10.1016/j.agrformet.2019.107786>,
670 2020.

671 Peel, M. C., Finlayson, B. L., and McMahon, T. A.: Updated world map of the Köppen-Geiger
672 climate classification, 11, 1633–1644, <https://doi.org/10.5194/hess-11-1633-2007>, 2007.

673 [Rigden, A. J. and Salvucci, G. D.: Evapotranspiration based on equilibrated relative humidity](#)
674 [\(ETRHEQ\): Evaluation over the continental U.S., 51, 2951–2973,](#)
675 <https://doi.org/10.1002/2014WR016072>, 2015.

676 Sahoo, A. K., Pan, M., Troy, T. J., Vinukollu, R. K., Sheffield, J., and Wood, E. F.: Reconciling the
677 global terrestrial water budget using satellite remote sensing, *Remote Sensing of Environment*, 115,
678 1850–1865, <https://doi.org/10.1016/j.rse.2011.03.009>, 2011.

679 Sándor, R., Barcza, Z., Hidy, D., Lellei-Kovács, E., Ma, S., and Bellocchi, G.: Modelling of grassland
680 fluxes in Europe: Evaluation of two biogeochemical models, *Agriculture, Ecosystems &*
681 *Environment*, 215, 1–19, <https://doi.org/10.1016/j.agee.2015.09.001>, 2016.

682 Shi, H., Hellwich, O., Luo, G., Chen, C., He, H., Ochege, F. U., Van de Voorde, T., Kurban, A., and
683 de Maeyer, P.: A global meta-analysis of soil salinity prediction integrating satellite remote sensing,
684 soil sampling, and machine learning, 1–15, <https://doi.org/10.1109/TGRS.2021.3109819>, 2021.

685 [Shi, H., Luo, G., Hellwich, O., Xie, M., Zhang, C., Zhang, Y., Wang, Y., Yuan, X., Ma, X., and](#)
686 [Zhang, W.: Variability and Uncertainty in Flux-Site Scale Net Ecosystem Exchange Simulations](#)
687 [Based on Machine Learning and Remote Sensing: A Systematic Evaluation, *Biogeosciences*](#)
688 [Discussions, 1–25, 2022.](#)

689 Tramontana, G., Jung, M., Schwalm, C. R., Ichii, K., Camps-Valls, G., Ráduly, B., Reichstein, M.,
690 Arain, M. A., Cescatti, A., Kiely, G., Merbold, L., Serrano-Ortiz, P., Sickert, S., Wolf, S., and Papale,
691 D.: Predicting carbon dioxide and energy fluxes across global FLUXNET sites with regression
692 algorithms, *Biogeosciences*, 13, 4291–4313, <https://doi.org/10.5194/bg-13-4291-2016>, 2016.

693 Van Hulse, J., Khoshgoftaar, T. M., and Napolitano, A.: Experimental perspectives on learning from
694 imbalanced data, in: Proceedings of the 24th international conference on Machine learning, New
695 York, NY, USA, 935–942, <https://doi.org/10.1145/1273496.1273614>, 2007.

696 Van Wijk, M. T. and Bouten, W.: Water and carbon fluxes above European coniferous forests
697 modelled with artificial neural networks, [https://doi.org/10.1016/S0304-3800\(99\)00101-5](https://doi.org/10.1016/S0304-3800(99)00101-5), 1999.

698 Virkkala, A.-M., Aalto, J., Rogers, B. M., Tagesson, T., Treat, C. C., Natali, S. M., Watts, J. D.,
699 Potter, S., Lehtonen, A., Mauritz, M., Schuur, E. A. G., Kochendorfer, J., Zona, D., Oechel, W.,
700 Kobayashi, H., Humphreys, E., Goeckede, M., Iwata, H., Lafleur, P. M., Euskirchen, E. S., Bokhorst,
701 S., Marushchak, M., Martikainen, P. J., Elberling, B., Voigt, C., Biasi, C., Sonnentag, O., Parmentier,
702 F.-J. W., Ueyama, M., Celis, G., St.Louis, V. L., Emmerton, C. A., Peichl, M., Chi, J., Järveoja, J.,
703 Nilsson, M. B., Oberbauer, S. F., Torn, M. S., Park, S.-J., Dolman, H., Mammarella, I., Chae, N.,
704 Poyatos, R., López-Blanco, E., Christensen, T. R., Kwon, M. J., Sachs, T., Holl, D., and Luoto, M.:
705 Statistical upscaling of ecosystem CO₂ fluxes across the terrestrial tundra and boreal domain:

设置了格式: 字体: 11 磅

设置了格式: 字体: 11 磅

设置了格式: 字体: 11 磅

706 Regional patterns and uncertainties, *Global Change Biology*, 27, 4040–4059,
707 <https://doi.org/10.1111/gcb.15659>, 2021.

708 Wagle, P., Bhattarai, N., Gowda, P. H., and Kakani, V. G.: Performance of five surface energy
709 balance models for estimating daily evapotranspiration in high biomass sorghum, *ISPRS Journal of*
710 *Photogrammetry and Remote Sensing*, 128, 192–203, <https://doi.org/10.1016/j.isprsjprs.2017.03.022>,
711 2017.

712 [Walther, S., Besnard, S., Nelson, J. A., El Madany, T. S., Migliavacca, M., Weber, U., Ermida, S. L., Brümmer,](#)
713 [C., Schrader, F., Prokushkin, A. S., Panov, A. V., and Jung, M.: Technical note: A view from space on global](#)
714 [flux towers by MODIS and Landsat: The FluxnetEO dataset, 1–40, <https://doi.org/10.5194/bg-2021-314>, 2021.](#)

715 Xie, M., Luo, G., Hellwich, O., Frankl, A., Zhang, W., Chen, C., Zhang, C., and De Maeyer, P.:
716 Simulation of site-scale water fluxes in desert and natural oasis ecosystems of the arid region in
717 Northwest China, 35, e14444, <https://doi.org/10.1002/hyp.14444>, 2021.

718 Xu, T., Guo, Z., Liu, S., He, X., Meng, Y., Xu, Z., Xia, Y., Xiao, J., Zhang, Y., Ma, Y., and Song, L.:
719 Evaluating Different Machine Learning Methods for Upscaling Evapotranspiration from Flux Towers
720 to the Regional Scale, 123, 8674–8690, <https://doi.org/10.1029/2018JD028447>, 2018.

721 Yang, F., White, M. A., Michaelis, A. R., Ichii, K., Hashimoto, H., Votava, P., Zhu, A.-X., and
722 Nemani, R. R.: Prediction of Continental-Scale Evapotranspiration by Combining MODIS and
723 AmeriFlux Data Through Support Vector Machine, 44, 3452–3461,
724 <https://doi.org/10.1109/TGRS.2006.876297>, 2006.

725 Zeng, J., Matsunaga, T., Tan, Z.-H., Saigusa, N., Shirai, T., Tang, Y., Peng, S., and Fukuda, Y.:
726 Global terrestrial carbon fluxes of 1999–2019 estimated by upscaling eddy covariance data with a
727 random forest, 7, <https://doi.org/10.1038/s41597-020-00653-5>, 2020.

728 [Zeng, Y., Hao, D., Huete, A., Dechant, B., Berry, J., Chen, J. M., Joiner, J., Frankenberg, C., Bond-](#)
729 [Lamberty, B., Ryu, Y., Xiao, J., Asrar, G. R., and Chen, M.: Optical vegetation indices for monitoring](#)
730 [terrestrial ecosystems globally, *Nat Rev Earth Environ.* 1–17, \[https://doi.org/10.1038/s43017-022-\]\(https://doi.org/10.1038/s43017-022-00298-5\)](#)
731 [00298-5](#), 2022.

732 Zhang, C., Luo, G., Hellwich, O., Chen, C., Zhang, W., Xie, M., He, H., Shi, H., and Wang, Y.: A
733 framework for estimating actual evapotranspiration at weather stations without flux observations by
734 combining data from MODIS and flux towers through a machine learning approach, *Journal of*
735 *Hydrology*, 603, 127047, <https://doi.org/10.1016/j.jhydrol.2021.127047>, 2021.

736 Zhang, K., Kimball, J. S., Nemani, R. R., and Running, S. W.: A continuous satellite-derived global
737 record of land surface evapotranspiration from 1983 to 2006, 46,
738 <https://doi.org/10.1029/2009WR008800>, 2010.

739 Zhao, W. L., Gentine, P., Reichstein, M., Zhang, Y., Zhou, S., Wen, Y., Lin, C., Li, X., and Qiu, G.
740 Y.: Physics-Constrained Machine Learning of Evapotranspiration, 46, 14496–14507,
741 <https://doi.org/10.1029/2019GL085291>, 2019.

设置了格式: 字体: 11 磅

设置了格式: 字体: 11 磅

设置了格式: 字体: 11 磅

742
743